FULL PAPER

Mechanical Surface Modification of Lithium Metal: Towards Improved Li Metal Anode Performance by Directed Li Plating

Myung-Hyun Ryou, Yong Min Lee, Yunju Lee, Martin Winter, and Peter Bieker**

The effect of mechanical surface modification on the performance of lithium (Li) metal foil electrodes is systematically investigated. The applied micro-needle surface treatment technique for Li metal has various advantages. 1) This economical and efficient technique is able to cover a wide range of surface area with a simple rolling process, which can be easily conducted. 2) This technique achieves improved rate capability and cycling stability, as well as a reduced interfacial resistance. The micro-needle treatment improves the rate capability by 20% (0.750 mAh at a rate of 7C) and increases the cycling stability by 200% (85% of the initial discharge capacity after 150 cycles) compared to untreated bare Li metal (0.626 mAh at a rate of 7C, 85% of the initial discharge capacity after only 70 cycles). 3) This technique efficiently suppresses Li formation of high surface area Li during the Li deposition process, as preferred sites for controlled Li plating are generated.

1. Introduction

With increasing environmental concerns about the global warming caused by fossil fuels consumption and the rapid depletion of fossil fuels as well, there are various efforts to replace internal combustion engines with electric motors and develop electrical energy storage systems (EESSs).[1–4] In order to achieve these goals, new large-scale battery systems have to give high energy and power densities; long cycle life and low cost are further requirements. Although Li-ion batteries (LIBs) have been the dominating power sources of consumer portable electronic markets during the last two decades due to their overwhelming performance compared to other electrochemical battery systems,[5–10] at the moment they cannot fulfill all the requirements of large-scale applications.[11] In order to satisfy the needs of these applications, LIBs should realize much higher specific energies with lower price compared to present. Unfortunately, however, LIBs are facing an energy limitation as approaching their theoretical limit calculated by the electrode materials used,[12] closely associated with a general electrode-materials pool based on intercalation and insertion chemistry.[13–15] Alternative energy storage systems based on alternative chemistries such as metal/air batteries[2,5,11,12,16,17] and Li/sulfur (S) batteries[2,15,18,19] are intensively studied recently, as they theoretically show much higher specific energies (Wh kg^{-1}) than LIBs.

Among various metal/air batteries based on different materials including Zn, Fe, Na, Ca, Mg, Al, and Li, Li/air batteries seem to be most promising,[16,20] because they have the highest specific capacity and specific energy taking into account both oxygen and Li [1920 mAh g^{-1} and 5588 Wh kg^{-1} for $2Li + 1/2O_2 \leftrightarrow Li_2O$ assuming a cell voltage of 2.91V, 1166 mAh g^{-1} and 3615 Wh kg^{-1} for $2Li + O_2 \leftrightarrow Li_2O_2$ assuming a cell voltage of 2.96V, respectively][2,16,21] compared to other metal/air battery systems. Although the first Li/air batteries were reported in 1996 by Abraham and Jiang,[22] their practical implementation has a long way to go yet, because there are major technical challenges which include: 1) the limited reversibility of the air cathode,[23–26] 2) the chemically and electrochemically instable electrolyte under operation conditions,[27–30] and 3) the highly reactive nature of Li metal deteriorating performance and safety.[31–33] In order to develop optimized structured cathodes[23–26] and suitable electrolyte media,[27–30] there have been numerous studies on possible candidates and solutions.

Despite the plenty of reports on Li metal anodes dated back to the 1960s to 1980s, the efforts addressing the importance of the nature of the Li metal electrode itself and its surface properties before electrochemical application are seldom considered. For instance, unlike LIB anodes, such as graphite,[34,35] the surface morphology of the pristine Li metal anode and its preconditioning before electrochemical application has not found considerable attention.

Due to various advantages such as low redox potential (–3.04 V vs standard hydrogen electrode), high specific capacity (3860 mAh g^{-1}), and low atomic weight, Li metal still is a very attractive anode candidate.[6,8,14,36]

For a rechargeable Li metal anode with high performance and safety, the Li plating process should yield a smooth

Prof. M.-H. Ryou, Prof. Y. M. Lee, Y. Lee
Department of Chemical and Biological Engineering
Hanbat National University
Daejeon, 305–719, Republic of Korea
E-mail: mhryou@hanbat.ac.kr
Prof. M. Winter, Dr. P. Bieker
Institute of Physical Chemistry
MEET Battery Research Centre
University of Muenster, Corrensstraße 46
48149, Muenster, Germany
E-mail: peter.bieker@uni-muenster.de

DOI: 10.1002/adfm.201402953

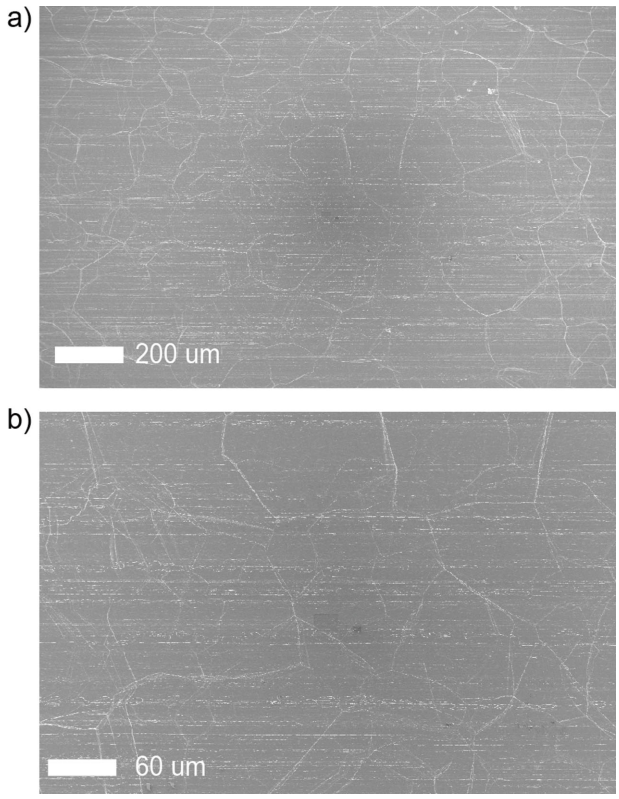

Figure 1. SEM images of the surface (top view) of the bare Li metal at various magnifications. Even Li metal, "fresh" from the roll, contains defects at the surface.

morphology. Non-uniform current density originated from any surface or solid electrolyte interphase (SEI)[6,14,53] will inevitably result in the formation of high surface area lithium (HSAL), with a mossy, dendritic or granular morphology. Even a pristine, fresh Li metal foil surface contains defects (**Figure 1**), which serve as nucleus for HSAL formation.[37,38] On the other hand, HSAL formation has a direct relation with the applied current density for plating and stripping.[39] Li metal shows reasonable plating/stripping efficiencies and lower HSAL formation tendency when the current density for the Li plating process is controlled at a low level.[14,39,40] In view of the fact that a low current density plays an important role in alleviating HSAL formation, attempts have been made to increase the active surface area, and thus to decrease the actual current density of the Li metal electrode in a physical manner, such as using Li metal powder.[41–48] Although a tangible improvement over Li metal foil is obtained, it must be noted that an additional complex and high-cost process is required to prepare Li powder based material and electrodes.

In this work, we suggest a simple, economical, and efficient micro-needle surface structural modification technique of Li metal foil inspired from skin needling (needle dermabrasion).

Skin needling has been introduced more than a decade ago, in the field of transdermal drug delivery,[49–51] and treatment of acne scars.[52,53] Micro-needles are perceived as an advanced pain-free technique for the penetration of several drugs including large molecular weight of drugs into the skin, which cannot be transported into the skin passively, and for skin treatment via wound healing process. Micro-needles are generally shorter than traditional needles, i.e., less than 1 mm long, but long enough to breach the stratum corneum barrier layer. They are able to create hundreds of micro-clefts covering large area of the skin at the same time, and suitable for low cost mass production.[54] In summary, skin needling is a well-known surface treatment technique for surface roughening and thus enhancing the "accessibility" of the surface, but has never been applied to Li metal anodes, so far.

The idea of this work is to introduce a higher surface area on the Li metal electrode that alleviates HSAL formation and in addition creates "defects by design", that serve as preferred Li plating sites. With this measure we aim to distribute and to locally direct the Li plating and stripping processes. The surface modification by the micro-needles is mechanically easy, due to the soft and ductile nature of Li.

2. Results and Discussions

2.1. Mechanical Surface Modification of Li Metal Foil using the Micro-Needle Technique

Micro-needles with diverse geometries made of various materials, such as metal, silicon, carbohydrates, and polymers using various micro-fabrication techniques, have been commercially available for skin care purpose.[49,50,54] In this study, we used a micro-needle roller based on the bio-degradable polymer material, polylactide, which is environmentally friendly and economic as well. The micro-needle roller is composed of a handle and a roller head (**Figure 2**a). As illustrated in Figure 2b and 2c, the roller head contains 20 lines of 200 μm length micro-needle arrays and thus can simply produce 340 micro-needle patterns during only one rotation of the roller head. In order to achieve evenly distributed micro-needle patterns on the Li metal surfaces, we gently rolled the roller over the Li metal surfaces as illustrated in **Figure 3**a and repeated this procedure for several times with different directions in a perpendicular direction and a slanted direction as described in Figure 3b and 3c.

Figure 4 demonstrates the morphological changes of the Li metal surfaces using scanning electron microscopy (SEM) after the micro-needle surface treatment. Figure 4a–4c are top view SEM images of the Li metal surfaces and Figure 4d–4f are cross-section images of the Li metal foil. Figure 1 is top view SEM images of the bare Li metal surfaces for com-

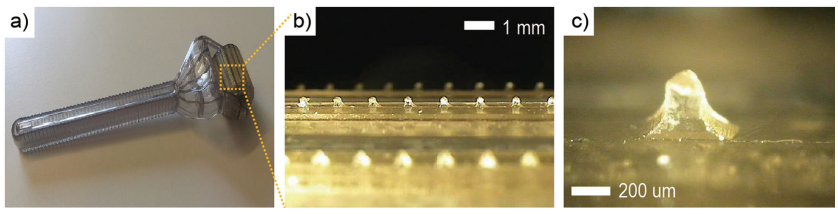

Figure 2. a) A digital image of the micro-needle roller. b) An optical microscopy (OM) picture of the roller head and c) a high-resolution OM image of the micro-needle shown in Figure 2b.

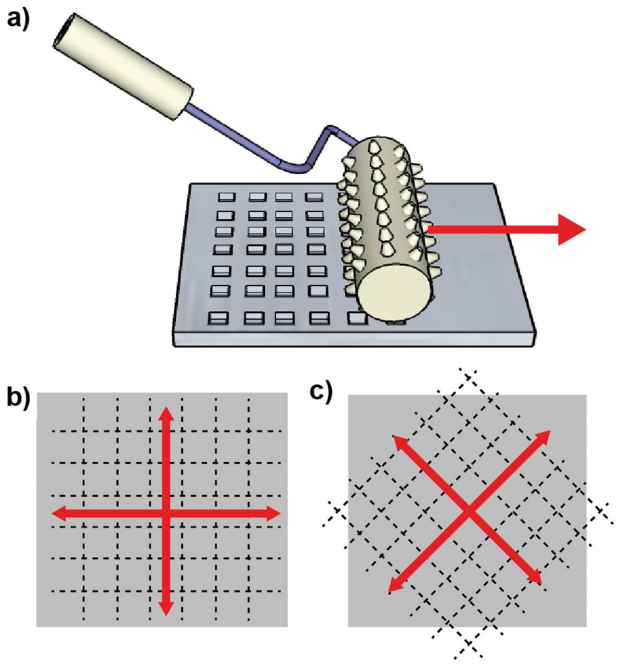

Figure 3. Schematic figures illustrating the micro-needle technique. a) An overview of the micro-needle technique creating surface patterns on the Li metal. Two successive rolling directions in b) a horizontal-vertical way and c) slanted way for creating the Li metal surface patterns.

parison. It was possible to "mirror" the inverse structure of the micro-needle on the Li metal surface using the micro-needle technique. There is little structural difference between the micro-needle mounted on the roller-head and the inverse micro-needle structure in the Li metal, indicating an easy mechanical deformation of the highly ductile ("soft") Li metal by the micro-needle treatment. As illustrated by Figure 4b and 4c, the surface structure of the deepest section of the hole, corresponding to tip of the micro-needle on the roller head, is relatively smooth. This is ascribed to the highest mechanical pressure, which was derived during the rolling procedure. Contrary to this and interestingly, as shown by Figure 4d, 4e and 4f, the surface structure of the hole walls represents vertical striations, which seem to be a result of the Li metal fracture during the treatment procedure. We could obtain identical structures over several repeated trials. In consequence, we can claim, that the micro-needle technique has several advantages in that it is relatively quick, quantitative and reproducible.

2.2. Impedance Measurements of Micro-Needle Treated Li Metal Foil

We measured the electrochemical-impedance-spectra (EIS) of LFP/Li metal cells in three-electrode configuration after the first cycle. As demonstrated in **Figure 5**, the overall impedance of the bare, untreated Li metal is much larger than the micro-needle-treated Li metal. This can be attributed to the fact that the surface area of the micro-needle treated Li metal is much larger than that of bare Li metal, while the electrodes have the same geometric dimension. The electrochemical reactions occur inevitably on/at the Li metal surface. Consequently, when the same amount of current is applied, the increase of Li metal surface area facilitates the electrochemical reaction rate at the Li metal surface and decreases the polarization of the Li electrode at the interface to the electrolyte.[43,55]

2.3. Polarization Behavior of Li/Li Symmetric Cells During Plating and Stripping

Along with the EIS results, the effect of the micro-needle treatment on the polarization process (Li stripping/plating) was investigated using Li/Li symmetric cells in three electrode configuration. **Figure 6** illustrates the potential-time profile during galvanostatic cycling. We applied a constant current (0.53 mA cm^{-2}) for the stripping/plating cycling steps and monitored potential changes as a function of time. The symmetric cells employing bare Li metal show a higher absolute value of overpotential compared to those of micro-needle treated

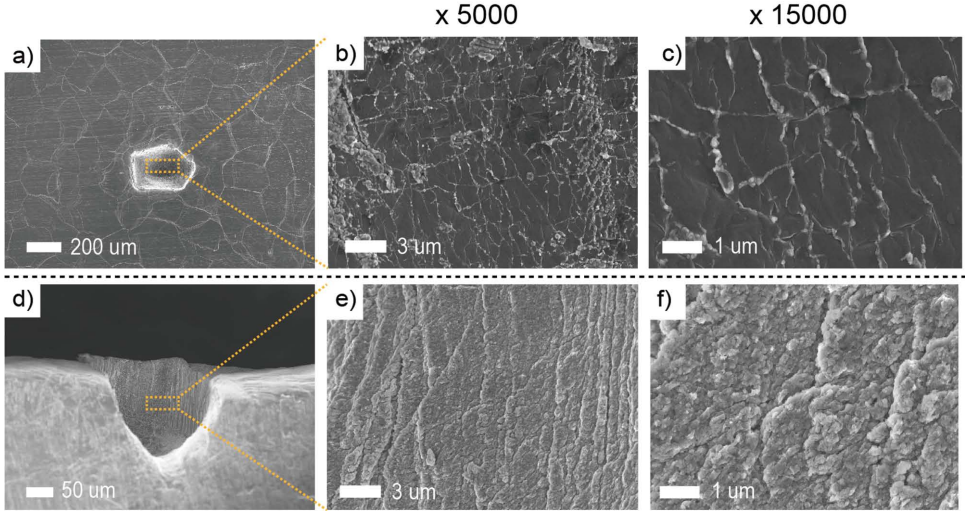

Figure 4. SEM images of a–c) the surface (top view) and d–f) the cross-section of the micro-needle treated Li metal.

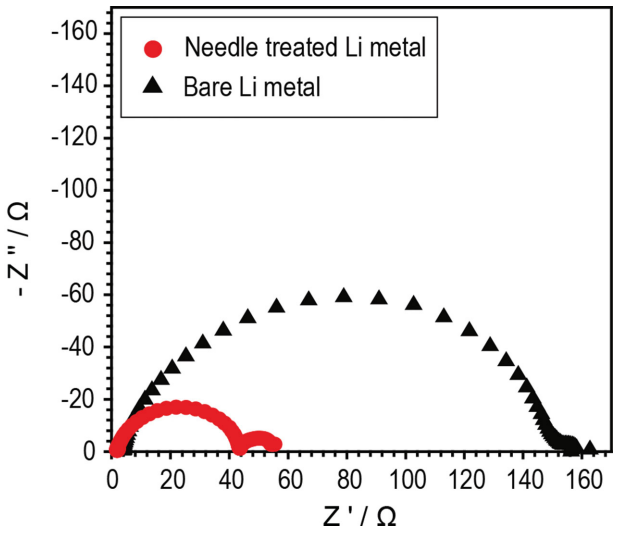

Figure 5. Nyquist plots of the Li half-cells after the first cycle measured at C/10 (0.1 mA cm^{-2}) rate between 2.0 and 4.2 V (vs Li/Li^+) at 25 °C [LFP/separator/Li metal with and without surface modification of Li metal using the micro-needle technique].

Li metal. When the cell performance stabilized after 150 h of cycling, the cells employing the bare Li metal revealed an overpotential of +0.06 V vs Li/Li^+ during the stripping steps, which is a ca. 200% higher value compared to the cells using Li metal after micro-needle treatment (+0.03 V vs Li/Li^+). Again, well associated with the impedance results described above, this implies that the bare Li metal shows a significantly higher resistance for the transfer Li ions and electrons during operation.

2.4. Cycling Performance of Micro-Needle Treated Li Metal

In order to elucidate the effect of micro-needle treatment on the cycling performance of Li metal anode, the cell performances of Li half-type cells consisting of LFP and Li metal with and without micro-needle treatment were investigated. In addition, we investigated the rate capabilities of the cells as a function of different current densities keeping the charge (= plating on Li) current densities at a C/2 rate (0.53 mA cm^{-2}) in **Figure 7**a. At the beginning of the experiments, when the discharge (= stripping of Li) current rate was as low as C/10 (0.1 mA cm^{-2}), the discharge capacities were almost similar for both cases. Whereas, as the discharge current rate increases over C/2, a gap between the discharge capacities arises and gets larger with increasing discharge current. For example, at a 7C rate (7.42 mA cm^{-2}) the cell with micro-needle treated Li metal achieved a 20% higher discharge capacity compared to bare Li metal (0.750 mAh for the micro-needle treated Li metal and 0.626 mAh for the bare Li metal). These results might be attributed to the higher surface area and unique morphology of the micro-needle treated Li metal.

In addition, we also investigated the effect of micro-needle treated Li metal on the discharge capacity cycling stability of the LFP/Li metal cells, operated at 25 °C at C/2 rate (0.53 mA cm^{-2}, Figure 7b). The micro-needle treated Li metal revealed a higher discharge capacity (1.18 mAh in the 1st cycle) and much

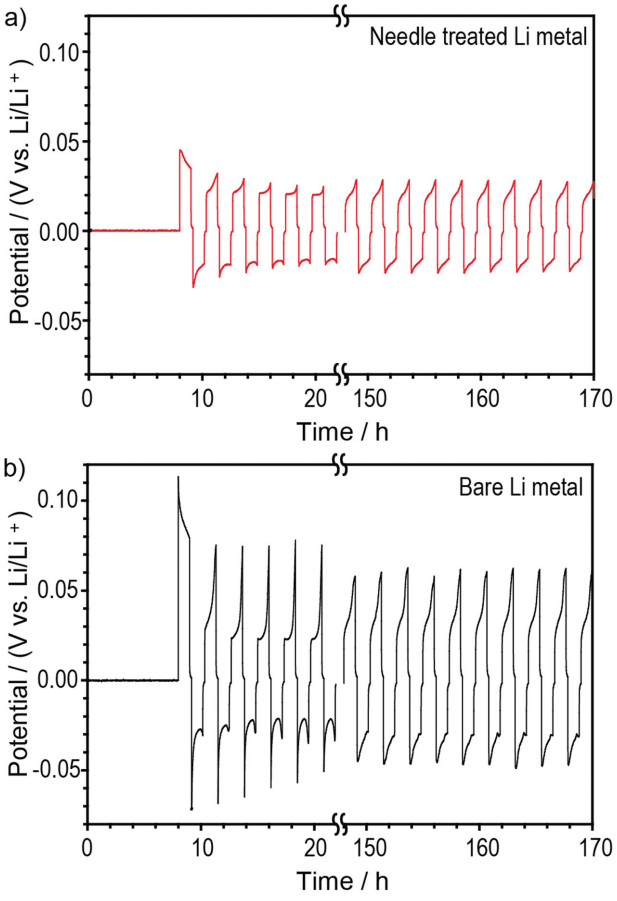

Figure 6. Potential profiles of Li/Li symmetric cells during galvanostatic cycling for a) needle treated Li metal and b) bare Li metal. The current density is 0.53 mA cm^{-2} for each stripping and plating step [+0.53 mA cm^{-2} (1 h) → Rest (10 min) → –0.53 mA cm^{-2} (1 h) → Rest (10 min)].

improved discharge retention abilities as well (85% of the initial discharge capacity after 150 cycles) compared to those of bare Li metal (1.14 mAh in the 1st cycle, 85% of the initial discharge capacity after 70 cycles). Furthermore, the bare Li metal severely deteriorates the discharge capacity even after 70 cycles. The results of rate capability experiments shown in Figure 7a support the higher discharge capacities of the micro-needle treated Li metal. On the other hand, current density plays a crucial role in determining the cycling performance. In general, the cycling stability of cells employing a Li metal electrode exponentially increases as the charge current density decreases,[14,39] because a small current density can effectively diminish the formation of HSAL. Along with this behavior, the micro-needle treated Li metal with a larger surface area is subjected to a lower actual charge current density compared to the bare Li metal under the same operation conditions and thus could achieve remarkably improved cycling stability and capacity retention.

Figure 8 displays the potential profiles for selected cycle numbers, 1st, 20th, 50th, 100th, and 150th, of the unit cells (LFP/Li metal) operated at a C/2 rate (0.53 mA cm^{-2}) demonstrated in Figure 7b. Note that there are severe potential differences between the charging/discharging processes in the bare Li metal case as the cycle number increases. This implies that cell

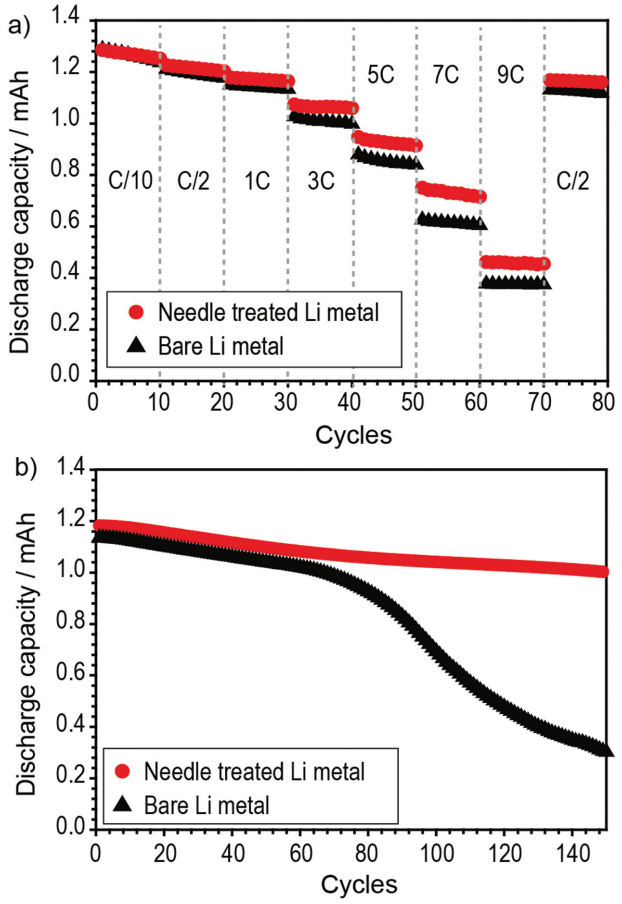

Figure 7. Electrochemical measurements of LFP/Li half-cells cells employing Li metal after and without micro-needle surface treatment. a) A comparison of the discharge capacities of the cells at different discharge rates while keeping the charge rate constant at C/2 (0.53 mA cm^{-2}). b) The cycling performance was measured at a C/2 rate (0.53 mA cm^{-2}) between 2.0 and 4.2 V (vs Li/Li^+).

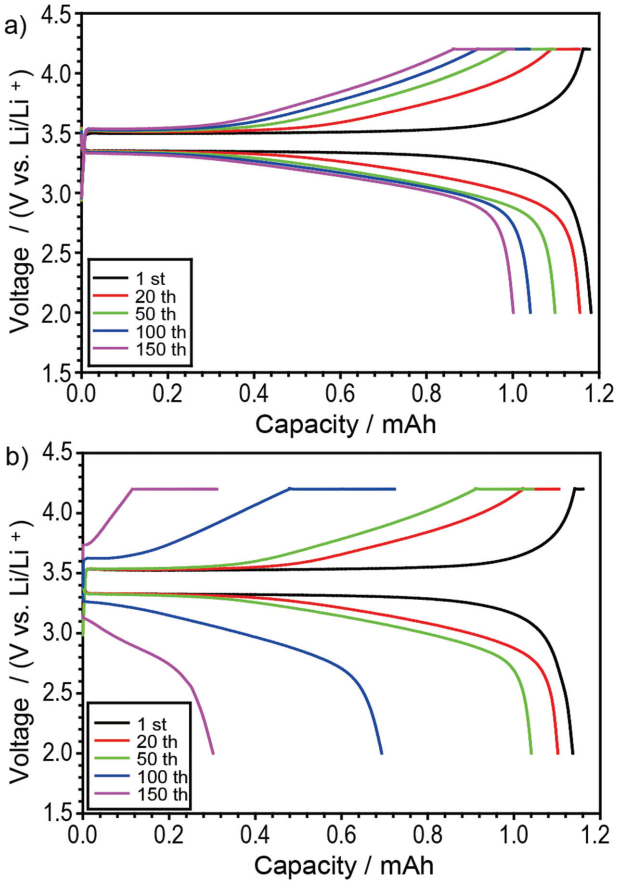

Figure 8. Potential profiles of LFP/Li half-cells during cell operation shown in Figure 7b, employing a) needle-treated Li metal and b) bare Li metal between 2.0 and 4.2 V (vs Li/Li^+) at a C/2 rate (0.53 mA cm^{-2}).

polarization of the bare Li metal is much larger compared to the micro-needle treated Li metal. The bigger electrode polarization of the bare Li metal (Figure 8), closely associated with larger impedance values in EIS results (Figure 5), also supports the findings of poor capacity retention and cycling stability shown in Figure 7b.

2.5. Morphology Changes of Micro-Needle Treated Li Metal After Cycling

In order to elucidate the effect of the micro-needle treatment on HSAL formation, structural changes of the Li metal surface after electrochemical operation were investigated using scanning electron microscopy (SEM). **Figure 9** displays SEM images of the Li metal surfaces with and without the micro-needle treatment after a Li plating process for 10 min. Compared to the SEM images of the bare micro-needle treated Li metal surfaces prior to the Li plating process displayed in Figure 4a, there are no significant differences in the SEM images of the surfaces except the point that small particles are deployed in places as shown in Figure 9a–c. The micro-needle pattern is well maintained and HSAL, usually formed on the Li metal surface after a polarization experiment,[37,56] are scarcely found. Contrary to this, the bare Li metal surface is full of small particles as shown in Figure 9d. Magnified SEM images of the bare Li metal electrode (Figure 9e and 9f) reveal the typical features of HSAL, such as Li dendrites.[14,39,40] Considering these results, the question comes up of how the Li is deposited on the micro-needle treated Li metal surface, to achieve a favorable deposition morphology.

In order to answer this question, we further investigated the morphological structure changes of the "hole-wall surfaces", by SEM (**Figure 10**). Comparing the SEM images of the hole wall surfaces before (Figure 4d–f) and after the Li plating process (Figure 10a–c), the original vertical striation pattern of hole wall surfaces became embossed, which implies that the Li is deposited alongside these unique wall structures in the hole. As a result, after the Li plating process, the structure of the hole-walls resembles that of a human/animal intestine, which surface structure and area is optimized for fast and efficient nutrient absorption. In other words with the unique morphology of the hole-wall surfaces, the Li deposition is preferably directed to these unique surfaces.

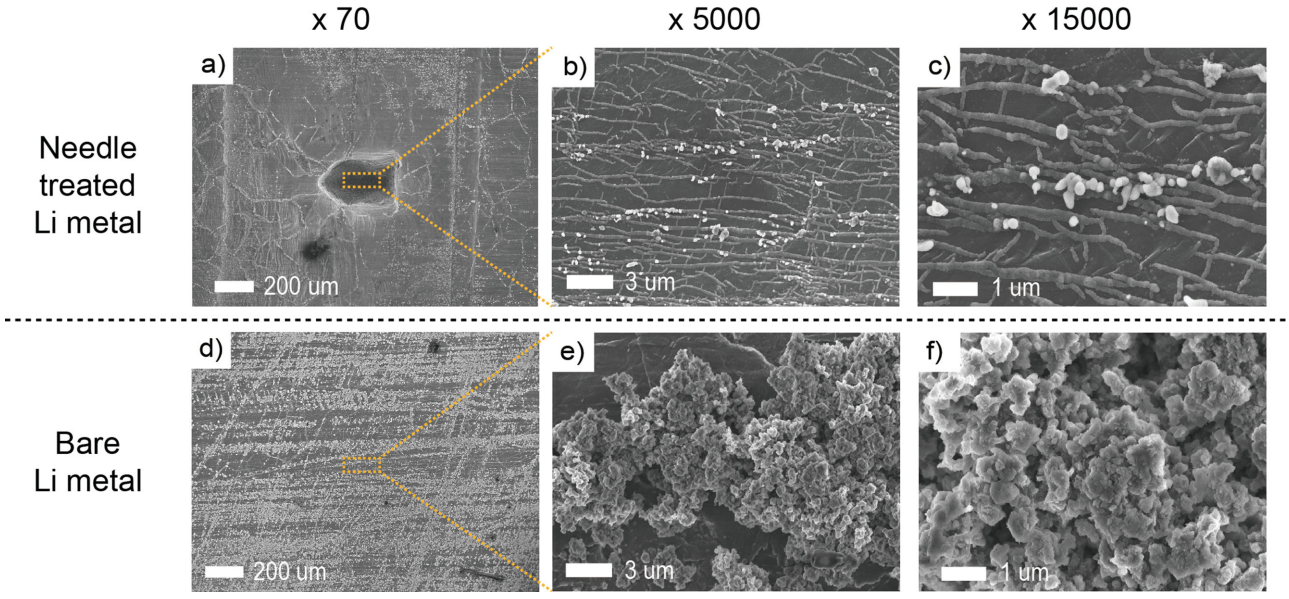

Figure 9. SEM images of the surfaces of a–c) the needle treated Li metal and d–f) the bare Li metal after polarization at 0.53 mA cm^{-2} for 10 min at different magnification.

Considering the SEM images, we suggest a plating mechanism on Li metal with and without the micro-needle treatment, respectively (**Figure 11**). On bare Li metal (Figure 11a), HSAL can be easily formed during the plating process (Figure 11b) due to an inhomogeneous charge transfer at the electrode/electrolyte interface, which is closely related with the inhomogeneous surface morphology and the inhomogeneous composition and structure of the solid electrolyte interphase (SEI).[6,14,57] For the micro-needle treated surface, the current distribution is different than on the untreated surface, so the lithium will plate inside the hole, starting at the unique wall surfaces and not on the plain, still bare lithium surface. This is, what we call locally directed Li plating. Until the holes are fully filled with Li, no plating on the still plain surface will take place and thus HSAL formation is delayed.

An associated effect can be related to the native layers of metallic Li. In general, Li metal is highly reactive and thus the Li metal surface is covered with native layers consisting of Li_2O, Li_2CO_3, and LiOH.[37,58] These layers consolidate during dry storage of metallic Li and they act as an additional resistance for lithium ion transfer during plating and stripping. After mechanical impact via micro-needle treatment, the native layers will be inevitably modified or even partially removed. In our mechanistic model, we subdivide the needle treated Li (Figure 11c) in three surface regions A, B, and C (Figure 11d). Contrary to the surface regions A and B, we believe that region C is not covered with the original native layers because these surfaces have experienced the micro-needle treatment leading to the rough hole-wall surface morphology with diminished or removed native surface layers. Consequently, region C has a lower resistance for charge transfer compared to the regions A and B and thus Li deposition can be faster on areas within region C than on areas of regions A and B, where the native layers are still in their original state. In summary, Li deposition is locally directed towards region C. Moreover, the larger surface area of region C attributed to their unique intestine-type vertical striation pattern has an advantage in that it can effectively reduce the actual current density, thus alleviating HSAL formation and growth.

3. Conclusion

In contrast to Li^+ insertion anode materials (such as graphite or $Li_4Ti_5O_{12}$ with insertion sites), the sites for charge storage of a Li metal foil electrode (the plating sites) will never be

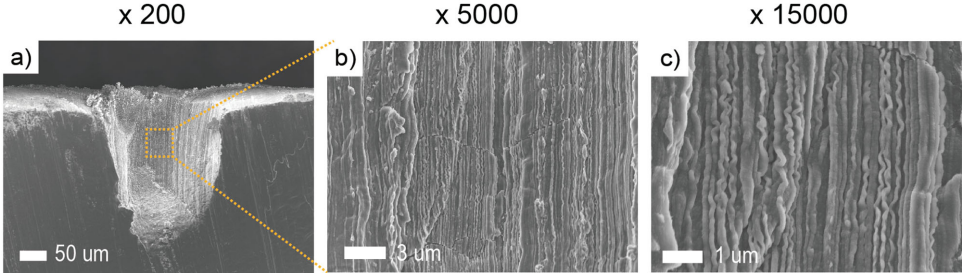

Figure 10. SEM images of the cross-section of needle treated Li metal after polarization at 0.53 mA cm^{-2} for 10 min at different magnification.

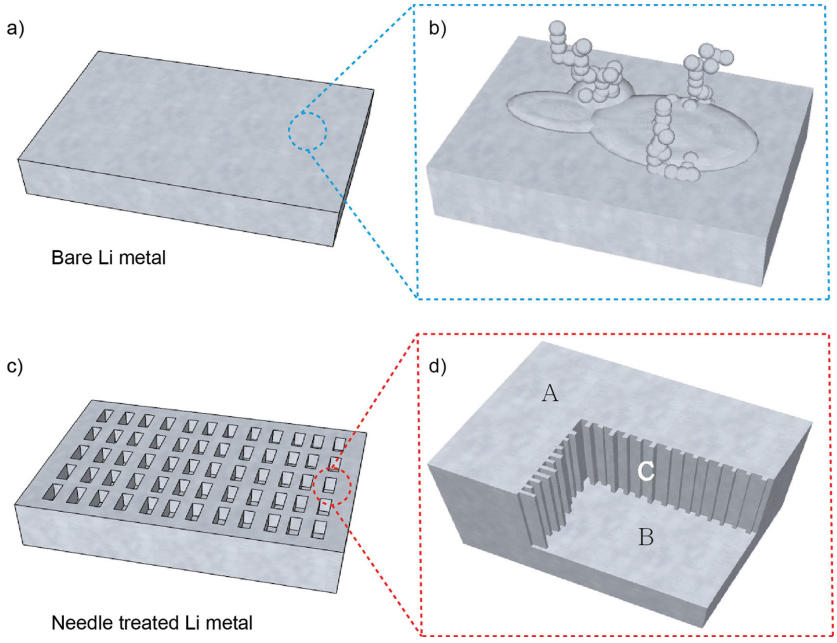

Figure 11. Schematic illustrations describing the Li plating mechanism on a,b) bare Li metal and c,d) micro-needle treated Li metal. Note that parts (b) and (d) are magnified images of the parts (a) and (b), respectively.

equivalent. This inevitably leads to inhomogeneous Li deposits (high surface area lithium, HSAL), which results in an inhomogeneous reactivity with the electrolyte. The formation of HSAL depends not only on surface composition and morphology, but also on the electrochemical conditions. Higher current leads to a greater amount of HSAL. The HSAL morphology will change from cycle to cycle and thus we see a strong development of the overpotentials on the local surface.

We suggest step back from the approach to aim at the Li electrode with a homogeneous surface and instead to direct and control the Li deposition process by introducing surface patterns favorable for Li deposition. A simple and economical micro-needle pre-treatment technique for Li metal foil was introduced as example of this new strategy, and the effect of this technique on the cell performance of a rechargeable Li metal electrode was systemically investigated. Using the micro-needle roller technique, we could successfully duplicate large numbers of inverse micro-needle structures over a wide area of the Li metal. The micro-needle patterns revealed a unique surface structure resembling to the inner structure of human/animal intestines, which means that the active surface area was effectively increased. The charge transfer resistance of the micro-needle treated Li metal was significantly reduced, and consequently the cycling performances of cells deploying the micro-needle treated Li metal were largely improved compared to bare Li metal. Considering the simplicity and effectiveness of this technique, we believe that the micro-needle surface modification technique will be a great step forward for realizing large-scale batteries employing a rechargeable Li metal electrode, such as Li/air and Li/S batteries, especially when deployed with other measures for suppression of HSAL, e.g., new electrolytes. Moreover, these promising results motivate us to apply other surface modification techniques. At the end, we like to emphasize, that the stripping/plating experiments in this work have been performed with a standard battery electrolyte and with non-optimized cycling regimes or cell configurations, thus opening the field for further improvements.

4. Experimental Section

Materials: Carbon-coated lithium iron phosphate ($LiFePO_4$, LFP, average particle size: 0.3 µm, carbon content: 2.3 wt%, Clariant, Germany), polyvinylidene difluoride (PVdF, Kynar FLEX 761A, Arkema Group), conductive agent (carbon black Super C65, Imerys), Li metal (thickness: 500 µm, Rockwood Lithium), and dimethyl carbonate (DMC, >99%, Aldrich) were used without purification. A mixture of ethylene carbonate/diethyl carbonate (EC:DEC = 1:1 by volume) containing 1M lithium hexafluorophosphate ($LiPF_6$) were purchased from Ube Industries Ltd. and used without further purification. Unless otherwise stated, this mixture is used as a liquid electrolyte during the electrochemical experiments. Whatman GF/D fiber separator was dried at 200 °C for 24 h under vacuum prior to use. The micro-needle roller (Mi-Roll, Daesung Medical Co. Ltd., Korea) was purchased.

Electrode Preparation: The electrode was prepared by casting a deionized (DI) water based slurry (LFP/PVdF/Super C65 = 90/5/5, w/w/w) onto aluminum foil with a 150 µm gap by the doctor blade technique. The electrode was dried at 110 °C for 24 h under vacuum prior to use. The diameter of the electrode was 12 mm and the mass loading was approximately 7.5 mg cm^{-2}.

Preparation of the Electrochemical Cells: The cells were assembled in Swagelok configurations. In all cells, glass fiber was deployed as a separator. 150 µL of liquid electrolyte were used for activation of the cells. All the procedures were conducted in a glove box filled with argon. For the Li/Li symmetric cells, a three-electrode configuration has been used, where Li metal was used both as a working, counter and as reference electrode, respectively. Li plating/stripping experiments were conducted at a current density of 0.53 mA cm^{-2}. The rest time between the Li plating and stripping process was 10 min in order to alleviate the influence of concentration gradients. Potential changes were monitored based on the reference Li electrode. Electrochemical impedance spectroscopy (EIS) was measured at room temperature with a Solartron SI 1287 potentiostat in combination with a Solartron SI 1260 impedance/gain-phase analyzer. The spectra were detected between 1 mHz and 1 MHz with an amplitude of 5 mV. In order to investigate the surface of the lithium electrodes, after the constant current cycling experiments, the Swagelok cells were disassembled. The sample electrodes were dried under vacuum and transferred into the scanning electron microscope (SEM) in a sealed vessel. SEM was measured with an Auriga field emission (FE)-SEM Crossbeam Workstation by Carl Zeiss with an acceleration voltage of 3 kV. A two electrode cell configuration was used for the cycling and rate performance measurement. LFP was used as a positive electrode and Li metal as negative electrode. The LFP/Li cells were pre-cycled in a voltage range between 2.0 and 4.2 at a constant current rate of 0.1 mA cm^{-2} for both the charge and the discharge process, and then cycled with different current densities (a constant current-constant voltage mode during the charging process and a constant current mode during the discharging process).

Scanning Electron Microscopy (SEM) Analysis: After electrochemical investigations, the cells were carefully disassembled in a dry glove box filled with argon. Samples were gently washed with DMC for several times and fully dried under vacuum for 24 h. In order to measure the

cross-section images of Li metal, we cut the Li metal samples with a sharp razor blade.

Supporting Information

Supporting Information is available from the Wiley Online Library or from the author.

Acknowledgements

M.-H. Ryou and Y. M. Lee contributed equally to this work. The authors wish to thank the German Ministry of Education and Research (BMBF) for funding of this work in the project "MEET-HiEnd" (03×4634A). We gratefully acknowledge the supply of materials by IMERYS.

Received: August 26, 2014
Revised: October 31, 2014
Published online: December 2, 2014

[1] C. Liu, F. Li, L. P. Ma, H. M. Cheng, *Adv. Mater.* **2010**, *22*, E28.
[2] B. Scrosati, J. Hassoun, Y.-K. Sun, *Energy Environ. Sci.* **2011**, *4*, 3287.
[3] G. Jeong, Y.-U. Kim, H. Kim, Y.-J. Kim, H.-J. Sohn, *Energy Environ. Sci.* **2011**, *4*, 1986.
[4] R. Wagner, N. Preschitschek, S. Passerini, J. Leker, M. Winter, *J. Appl. Electrochem.* **2013**, *43*, 481.
[5] J. S. Lee, S. Tai Kim, R. Cao, N. S. Choi, M. Liu, K. T. Lee, J. Cho, *Adv. Energy Mater.* **2011**, *1*, 34.
[6] J.-M. Tarascon, M. Armand, *Nature* **2001**, *414*, 359.
[7] J. Hassoun, P. Reale, B. Scrosati, *J. Mater. Chem.* **2007**, *17*, 3668.
[8] B. Dunn, H. Kamath, J.-M. Tarascon, *Science* **2011**, *334*, 928.
[9] J. O. Besenhard, M. Winter, *Pure Appl. Chem.* **1998**, *70*, 603.
[10] M.-H. Ryou, Y. M. Lee, J. K. Park, J. W. Choi, *Adv. Mater.* **2011**, *23*, 3066.
[11] M. Park, H. Sun, H. Lee, J. Lee, J. Cho, *Adv. Energy Mater.* **2012**, *2*, 780.
[12] J. Xiao, D. Mei, X. Li, W. Xu, D. Wang, G. L. Graff, W. D. Bennett, Z. Nie, L. V. Saraf, I. A. Aksay, *Nano Lett.* **2011**, *11*, 5071.
[13] X.-P. Gao, H.-X. Yang, *Energy Environ. Sci.* **2010**, *3*, 174.
[14] M.-H. Ryou, D. J. Lee, J. N. Lee, Y. M. Lee, J. K. Park, J. W. Choi, *Adv. Energy Mater.* **2012**, *2*, 645.
[15] X. Ji, L. F. Nazar, *J. Mater. Chem.* **2010**, *20*, 9821.
[16] X.-h. Yang, Y.-y. Xia, *J. Solid State Electrochem.* **2010**, *14*, 109.
[17] D. J. Lee, H. Lee, J. Song, M.-H. Ryou, Y. M. Lee, H.-T. Kim, J.-K. Park, *Electrochem. Commun.* **2014**, *40*, 45.
[18] L. Xiao, Y. Cao, J. Xiao, B. Schwenzer, M. H. Engelhard, L. V. Saraf, Z. Nie, G. J. Exarhos, J. Liu, *Adv. Mater.* **2012**, *24*, 1176.
[19] T. Greszler, M. Mathias, S. G. W. Gu, B. Lakshmanan, presented at Advanced Automotive Battery Conference, Pasadena, CA, February 2013.
[20] D. Egan, C. Ponce de León, R. Wood, R. Jones, K. Stokes, F. Walsh, *J. Power Sources* **2013**, *236*, 293.
[21] J. Christensen, P. Albertus, R. S. Sanchez-Carrera, T. Lohmann, B. Kozinsky, R. Liedtke, J. Ahmed, A. Kojic, *J. Electrochem. Soc.* **2011**, *159*, R1.
[22] K. Abraham, Z. Jiang, *J. Electrochem. Soc.* **1996**, *143*, 1.
[23] Y.-C. Lu, H. A. Gasteiger, Y. Shao-Horn, *J. Am. Chem. Soc.* **2011**, *133*, 19048.
[24] E. Yoo, H. Zhou, *ACS Nano* **2011**, *5*, 3020.
[25] Y.-C. Lu, Z. Xu, H. A. Gasteiger, S. Chen, K. Hamad-Schifferli, Y. Shao-Horn, *J. Am. Chem. Soc.* **2010**, *132*, 12170.
[26] R. Padbury, X. Zhang, *J. Power Sources* **2011**, *196*, 4436.
[27] Y. Chen, S. A. Freunberger, Z. Peng, F. Bardé, P. G. Bruce, *J. Am. Chem. Soc.* **2012**, *134*, 7952.
[28] H.-G. Jung, J. Hassoun, J.-B. Park, Y.-K. Sun, B. Scrosati, *Nat. Chem.* **2012**, *4*, 579.
[29] W. Xu, J. Hu, M. H. Engelhard, S. A. Towne, J. S. Hardy, J. Xiao, J. Feng, M. Y. Hu, J. Zhang, F. Ding, *J. Power Sources* **2012**.
[30] C. Laoire, S. Mukerjee, E. J. Plichta, M. A. Hendrickson, K. Abraham, *J. Electrochem. Soc.* **2011**, *158*, A302.
[31] J. Hassoun, H.-G. Jung, D.-J. Lee, J.-B. Park, K. Amine, Y.-K. Sun, B. Scrosati, *Nano Lett.* **2012**, *12*, 5775.
[32] J. O. Besenhard, M. Winter, *Chem. Phys. Chem.* **2002**, *3*, 155.
[33] T. Schedlbauer, S. Krüger, R. Schmitz, R. Schmitz, C. Schreiner, H. Gores, S. Passerini, M. Winter, *Electrochim. Acta* **2013**, *92*, 102.
[34] H. Buqa, P. Golob, M. Winter, J. Besenhard, *J. Power Sources* **2001**, *97*, 122.
[35] H. Buqa, R. Blyth, P. Golob, B. Evers, I. Schneider, M. S. Alvarez, F. Hofer, F. Netzer, M. Ramsey, M. Winter, *Ionics* **2000**, *6*, 172.
[36] M. Winter, J. O. Besenhard, *Chem. Unserer Zeit* **1999**, *33*, 252.
[37] L. Gireaud, S. Grugeon, S. Laruelle, B. Yrieix, J.-M. Tarascon, *Electrochem. Commun.* **2006**, *8*, 1639.
[38] J. Besenhard, M. Wagner, M. Winter, A. Jannakoudakis, P. Jannakoudakis, E. Theodoridou, *J. Power Sources* **1993**, *44*, 413.
[39] D. Aurbach, E. Zinigrad, Y. Cohen, H. Teller, *Solid State Ionics* **2002**, *148*, 405.
[40] F. Orsini, A. Du Pasquier, B. Beaudoin, J. Tarascon, M. Trentin, N. Langenhuizen, E. De Beer, P. Notten, *J. Power Sources* **1998**, *76*, 19.
[41] J. S. Kim, W. Y. Yoon, K. Y. Yi, B. K. Kim, B. W. Cho, *J. Power Sources* **2007**, *165*, 620.
[42] I. W. Seong, C. H. Hong, B. K. Kim, W. Y. Yoon, *J. Power Sources* **2008**, *178*, 769.
[43] C. Kwon, S. Cheon, J. Song, H. Kim, K. Kim, C. Shin, S. Kim, *J. Power Sources* **2001**, *93*, 145.
[44] B. B. Fitch, M. Yakovleva, Y. Li, I. Plitz, A. Skrzypczak, F. Badway, G. Amatucci, Y. Gao, *ECS Trans.* **2007**, *3*, 15.
[45] J. Heine, S. Krüger, C. Hartnig, U. Wietelmann, M. Winter, P. Bieker, *Adv. Energy Mater.* **2014**, *4*, 1300815.
[46] J. S. Kim, W. Y. Yoon, *Electrochim. Acta* **2004**, *50*, 531.
[47] J. S. Kim, S. hoon Baek, W. Y. Yoon, *J. Electrochem. Soc.* **2010**, *157*, A984.
[48] Y. S. Lee, J. H. Lee, J. Choi, W. Y. Yoon, D. W. Kim, *Adv. Funct. Mater.* **2013**, *23*, 1019.
[49] S. M. Bal, A. C. Kruithof, R. Zwier, E. Dietz, J. A. Bouwstra, J. Lademann, M. C. Meinke, *J. Controlled Release* **2010**, *147*, 218.
[50] R. F. Donnelly, M. J. Garland, D. I. Morrow, K. Migalska, T. R. R. Singh, R. Majithiya, A. D. Woolfson, *J. Controlled Release* **2010**, *147*, 333.
[51] S. Henry, D. V. McAllister, M. G. Allen, M. R. Prausnitz, *J. Pharm. Sci.* **1998**, *87*, 922.
[52] T. Leheta, A. El Tawdy, R. Abdel Hay, S. Farid, *Dermatol. Surg.* **2011**, *37*, 207.
[53] G. Fabbrocini, N. Fardella, A. Monfrecola, I. Proietti, D. Innocenzi, *Clin. Exp. Dermatol.* **2009**, *34*, 874.
[54] J.-H. Park, S.-O. Choi, S. Seo, Y. B. Choy, M. R. Prausnitz, *Eur. J. Pharm. Biopharm.* **2010**, *76*, 282.
[55] W.-S. Kim, W.-Y. Yoon, *Electrochim. Acta* **2004**, *50*, 541.
[56] J.-i. Yamaki, S.-i. Tobishima, K. Hayashi, K. Saito, Y. Nemoto, M. Arakawa, *J. Power Sources* **1998**, *74*, 219.
[57] M. Winter, *Z. Phys. Chem.* **2009**, *223*, 1395.
[58] S. Shiraishi, K. Kanamura, Z. Takehara, *J. Appl. Electrochem.* **1999**, *29*, 867.